Accepted Manuscript

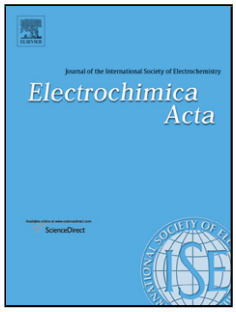

Title: Understanding the chemisorption-based activation mechanism of the oxygen reduction reaction on nitrogen-doped graphitic materials

Author: Adolfo Ferre-Vilaplana Enrique Herrero

PII: S0013-4686(16)30838-6
DOI: http://dx.doi.org/doi:10.1016/j.electacta.2016.04.039
Reference: EA 27074

To appear in: *Electrochimica Acta*

Received date: 24-12-2015
Revised date: 8-4-2016
Accepted date: 9-4-2016

Please cite this article as: Adolfo Ferre-Vilaplana, Enrique Herrero, Understanding the chemisorption-based activation mechanism of the oxygen reduction reaction on nitrogen-doped graphitic materials, Electrochimica Acta http://dx.doi.org/10.1016/j.electacta.2016.04.039

This is a PDF file of an unedited manuscript that has been accepted for publication. As a service to our customers we are providing this early version of the manuscript. The manuscript will undergo copyediting, typesetting, and review of the resulting proof before it is published in its final form. Please note that during the production process errors may be discovered which could affect the content, and all legal disclaimers that apply to the journal pertain.

ACCEPTED MANUSCRIPT

Understanding the chemisorption-based activation mechanism of the oxygen reduction reaction on nitrogen-doped graphitic materials.

Adolfo Ferre-Vilaplana[a] *and Enrique Herrero*[b]*

[a] *Instituto Tecnológico de Informática, Ciudad Politécnica de la Innovación, Camino de Vera s/n, E-46022 Valencia, Spain, and Departamento de Sistemas Informáticos y Computación, Escuela Politécnica Superior de Alcoy, Universidad Politécnica de Valencia, Plaza Ferrándiz y Carbonell s/n, E-03801 Alcoy, Spain.*

[b] *Instituto de Electroquímica, Universidad de Alicante, Apdo. 99, E-03080 Alicante, Spain. E-mail: herrero@ua.es*

Abstract.

To optimize nitrogen-doped graphitic materials as metal-free catalysts for the oxygen reduction reaction mechanisms have to be better understood. Here, the role played by pyridinic nitrogen-dopants in the chemisorption-based activation of the target reaction is revealed. The study is centered on the monodentate chemisorption of molecular oxygen as the first step of the process. Several configurations of nitrogen dopants in which there was always a nitrogen dopant in the edge of the material were tested using DFT. A clearly favorable chemisorbed state for molecular oxygen was found when the pyridinic nitrogen-dopant is hydrogenated and located at an armchair edge. The found chemisorbed state is further favored by additional available charge. By contrast, the chemisorbed state of oxygen is much less favorable when the hydrogenated pyridinic nitrogen-dopants are located at zigzag edges. Moreover, it was found that the charge involved in the hydrogenation of pyridinic nitrogen-dopants remains segregated, becoming available for reduction processes. Detailed reasons for the described facts are given, and an integrated model for the target activation mechanism is proposed including graphitic nitrogen-dopants effects.

ACCEPTED MANUSCRIPT

Keywords: Graphene; oxygen reduction reaction; nitrogen; edges.

1. Introduction.

Controlled oxidation of fuels in electrochemical cells is a promising energy conversion technology [1], whose future success depends on the development of an efficient catalyst for the oxygen reduction reaction (ORR). Platinum ORR catalysts have enabled the proof of concept but, mainly because of sluggish kinetics, cost and scarcity, low-platinum [2-5], non-platinum [6-9] and even metal-free [10-12] ORR catalysts are being investigated. Among these, nitrogen-doped graphitic materials exhibit activity towards the ORR [13-20]. However, the nature of the sites and the mechanisms explaining the observed activity are still under discussion. It has been suggested that the ORR on nitrogen-doped graphitic materials could take place without involving chemisorption [20]. However, without chemisorption, only hydrogen peroxide would be produced, which is an undesirable byproduct for fuel cell applications. Moreover, since the ORR is very sensitive to the surface structure and composition of the electrode, it is clear that chemisorbed species are always involved in the process. Thus, ORR mechanisms based on chemisorption have to be better understood to optimize the performance of these catalysts. In all the proposed mechanisms [16, 21] the first step in the reaction would give rise to a monodentate chemisorbed state of molecular oxygen, generally in the form of a superoxide. From that point, two possible scenarios arise. The first one considers the formation of adsorbed peroxide. Then, the reaction could yield hydrogen peroxide or evolve sequentially to water. In the other possible scenario, the adsorbed oxygen species would give rise to a bidentate configuration. From that, the oxygen-oxygen bond would be broken yielding finally water.

To determine the most probable mechanism, different facts and arguments can be considered. First, a significant production of hydrogen peroxide has been observed on nitrogen-

ACCEPTED MANUSCRIPT

doped graphitic materials [15, 17-18]. Second, the stabilizing solvation shell formed during the monodentate chemisorption of molecular oxygen [22] originates a significant barrier in order to evolve to the bidentate configuration. Finally, high activation energies for the cleavage of the oxygen-oxygen bond have been computed on these materials [16]. Moreover, the measured ORR activity on the investigated materials has been mainly attributed to the effect of graphitic [20] and pyridinic nitrogen dopants [19]. So, determining the role played by those dopants on graphitic materials to favor the monodentate chemisorption of molecular oxygen was established as the research goal. The evolution mechanisms from the investigated state to water [23] and optimal design strategies based on the adsorption energies of the intermediates [24] have been already reported.

To explain the ORR on nitrogen-doped graphitic materials, mechanisms involving graphitic nitrogen-dopants in the basal plane have been investigated [20, 23, 25-28]. However, a single nitrogen dopant or specific configurations of dopants in cluster have been usually considered. Motivated by the experimental visualization of unclustered graphitic nitrogen-dopants perfectly integrated in the graphene lattice [29], and by the fact that such a kind of defect has been identified as the one presenting the lowest energy [30], we explored recently the role played by unclustered graphitic nitrogen-dopants to activate oxygen in the basal plane [22]. In spite of the fact that the monodentate chemisorption of molecular oxygen on the basal plane of graphitic materials is usually considered as an unfavorable process [20], it was found that unclustered graphitic-nitrogen dopants would promote it, provided that two specific conditions are fulfilled. It was realized that the monodentate activation of molecular oxygen on graphitic materials requires of locally destabilized carbon atoms and globally available charge. The calculations demonstrated that graphitic nitrogen-dopants would be capable of playing both roles. So, it was shown that the monodentate chemisorption of molecular oxygen can take place on carbon atoms neighboring a graphitic nitrogen-dopant if, for instance, an additional graphitic

ACCEPTED MANUSCRIPT

nitrogen-dopant provides the required available charge. Moreover, solvation effects were found to be important in the mechanism, suggesting guidelines in order to capture it.

Regarding the ORR on the target materials, mechanisms involving pyridinic nitrogen-dopants at the edges have been also investigated [19, 31]. In fact, ORR activity on carbon atoms adjacent to pyridinic nitrogen-dopants has been recently demonstrated [19]. However, the microstructure and mechanisms have not been yet identified. We will provide computational evidence that the hydrogenation of pyridinic nitrogen-dopants could play a key role in the activation of molecular oxygen on nitrogen-doped graphitic materials. The hydrogenation [32] of pyridinic nitrogen-dopants in graphitic materials has been associated to high ORR activity in alkaline media. However, to our knowledge, no relevant role has been previously explicitly attributed to hydrogenated pyridinic nitrogen-dopants in explaining the activation of the ORR on the investigated materials. We will show that hydrogenated pyridinic nitrogen-dopants at armchair edges of graphitic materials can give rise to a clearly favorable monodentate chemisorbed state of molecular oxygen on their laterally adjacent carbon atoms. The found chemisorbed state would be further favored by additional available charge. By contrast, hydrogenated pyridinic nitrogen-dopants at zigzag edges would not be capable of so favorably activating oxygen on their adjacent carbon atoms. We will also show that the charge involved in the hydrogenation of pyridinic nitrogen-dopants remains segregated, becoming available for reduction processes. Moreover, detailed explanations for the described facts will be given and, considering also the role played by graphitic-nitrogen dopants, an integrated model for the target activation mechanism will be proposed.

2. Computational methods.

Mechanisms of the ORR on molecular and periodic models of nitrogen-doped graphitic materials have been previously investigated performing DFT calculations under the GGA

ACCEPTED MANUSCRIPT

approximation and using the PBE [33] functional [20, 23, 27, 30]. Thus, in this research, the monodentate chemisorption of molecular oxygen on nitrogen-doped graphitic materials was investigated using mainly different molecular models of nitrogen-doped graphene and performing DFT calculations under the GGA approximation and using the PBE functional and numerical basis sets of double-numerical plus polarization quality [34] as implemented in the Dmol^3 code [35]. Moreover, each one of the found fundamental effects was verified using also periodic models of armchair and zigzag nitrogen-doped graphene nanoribbons, and molecular models of armchair and zigzag nitrogen-doped single-walled carbon nanotubes. All the calculations were performed under neutral charge conditions. All the electrons were explicitly included in the calculations under a spin-unrestricted approach. Full and partial optimizations were carried out depending on the goal.

Since previous results [23] indicate that solvation effects are important in understanding the mechanisms, continuum solvation effects were taken into account by means of the COSMO model [36] and hydrogen bonds were captured by including additional explicit water molecules as solvation effect treatment [22]. To verify the quality of the selected solvation effect treatment, solvation energies were computed for oxygen and superoxide, obtaining values that were found to be consistent with those expected.

An orbital cutoff radius of 0.37 nm was used in the numerical basis set for all the atoms. The optimization convergence thresholds were set to 1.0×10^{-5} Ha for the energy, 0.02 Ha/nm for the force, and $5.0\text{x}10^{-4}$ nm for the displacement. The SCF convergence criterion was set to 1.0×10^{-6} Ha for the energy. A value of 78.54 was used as the dielectric constant in the continuous solvation model.

In order to capture hydrogen bonds, for models targeted to visualization (Figs. 3, 7, S2, S3, S5 and S7), an explicit water molecule was included in de model, in addition to the continuum solvation model, as solvation effect treatment. However, considering our previous

ACCEPTED MANUSCRIPT

results [22], for models targeted to energetics evaluations (Figs. 2, 6, 9 and S4) five explicit water molecules were included in the model, in addition to the continuum solvation model, as solvation effect treatment. A typical configuration of the formed explicit water solvation shell can be observed in Fig. S1.

Chemisorbed states were searched for running full optimizations. The relevance of each one of them was established determining its stability. For such a purpose, the energetics for the shortest distances of the reactions paths were estimated performing several constrained optimizations. For each reaction path, the basic configuration and treatment was maintained, but the distance between the carbon acting as active site and the nearest atom of the oxygen molecule was varied and constrained during the optimization process. To facilitate comparisons, the displayed total energies were referred to their respective references, calculated as the adsorbent energy plus that corresponding to the adsorbate complex in the bulk. Note that only relatively short C-O distances were considered. Thus, the final convergence to the alignment level of the respective references, at very long distances, is not displayed. The reasons for doing so were three. First, it has been pointed out that, because of the required change in the spin multiplicity, non-adiabatic effects could be implicated in the chemisorption of a solvated oxygen molecule. Second, for some of the considered cases, long distances between adsorbent and adsorbate give rise to very challenging models for which states of different spin multiplicity are very close in energy. Third, when solvation effects are sufficiently captured, the available charge of the surface is assigned to the solvated oxygen molecule during the optimization process, giving rise to a solvated superoxide anion, even when the oxygen molecule has not even yet come close to the surface. All these difficulties are circumvented by considering only relatively short C-O distances. For the shortest distances, the required spin multiplicity change has already taken place, the most favorable spin multiplicity of the solutions is much more clearly defined, and an eventual charge transfer to oxygen can be better explained.

ACCEPTED MANUSCRIPT

However, despite of only the shortest distances were considered, still useful insights can be derived about the investigated mechanism, for which detailed conceptual explanations will be provided.

All the calculations were run under automatic spin multiplicity conditions. For the adsorbate complex, formed by an oxygen molecule and five explicit water molecules in the bulk, triplet was found to be the most favorable spin multiplicity. For de rest of the models (adsorbents and those corresponding to each considered distance between adsorbent and adsorbate), for those having an even number of electrons, singlet was found to be the most favorable spin multiplicity, meanwhile, for those having an odd number of electrons, doublet was found to be the most favorable spin multiplicity. Therefore, along the considered distances, for each reaction path the most favorable spin multiplicity was found to be invariant.

Correcting results for dispersion forces was considered. Using the approach of Tkatchenko & Scheffler [37], but also the method of Grimme [38], it was estimated that such a kind of correction, for the investigated systems, would be of the order of 0.05 eV. Considering that the investigated reaction was chemisorption, for which significant energies in the order of 0.5 eV and higher were expected, we concluded that the considered correction could be safely neglected. For that reason, we decided not to correct our calculations, taking into account that dispersion forces are not always corrected by authors and that corrections for dispersion forces are not available in all the software packages.

3. Results and discussion.

As aforementioned, the first step in the investigated ORR mechanism would be the monodentate chemisorption of molecular oxygen on the material. In view of the figures displayed in a previous article [19], monodentate chemisorbed states of molecular oxygen on carbon atoms adjacent to pyridinic nitrogen-dopants at armchair edges were first considered.

ACCEPTED MANUSCRIPT

Thus, using a molecular model of graphene, several configurations of nitrogen dopants were explored, in which a pyridinic nitrogen-dopant was always included at an armchair edge (Fig. 1). The simpler one would be a single nitrogen dopant located at an armchair edge (Fig. 1A). For this configuration, the laterally neighboring carbon atom (labelled **a** in Fig.1) was initially tested for activation process. No significant chemisorbed state was found, as revealed by the energetics of the path shown in Fig. 2.

Trying to find a relevant monodentate chemisorbed state, an additional nitrogen dopant was included in the model, as shown in Fig. 1B. In our previous communication [22], the monodentate chemisorption of molecular oxygen on a carbon atom neighboring a graphitic nitrogen dopant required the presence of an additional graphitic nitrogen-dopant in the model. This additional nitrogen atom, which could be located even far away from the initial one, would supply the additional charge required for the stabilization of the chemisorbed oxygen molecule. However, unlike the case where two graphitic nitrogen dopants were included in the model [22], in this case (Fig. 1B), only a marginally stable chemisorbed state was found for the carbon atom labelled **a** (Fig. 2). In any case, the capability for contributing with charge of the graphitic nitrogen-dopant is also evidenced here, by the fact that the level of the energetic curve is displaced towards negative values. The charge that can be supplied from the region corresponding to the graphitic nitrogen-dopant can be transferred to oxygen, making possible the solvation of this adsorbed species. The generated solvation energy displaces the curve towards negative values because molecular oxygen in triplet state was used as the reference. The low stability of the observed state would be related to the fact that the carbon atom acting as the active site is not sufficiently destabilized.

However, when pyridinic nitrogen-dopants are incorporated to graphitic materials used as electrodes immersed in aqueous solutions, chemical reactions can take place, modifying the properties of the electrodes. Solvated pyridinic nitrogen have an acid-base equilibrium, which

ACCEPTED MANUSCRIPT

can be regarded as a proton adsorption/desorption process. Additionally, when a proton is adsorbed on a pyridinic nitrogen integrated in an electrode, the adsorbed positive charge can give rise to the transfer of an electron in a redox reaction to neutralize the positive charge. These two processes can be considered as a hydrogenation reaction. The situation is the same than that occurring on metallic electrodes, when platinum, palladium or iridium, adsorbs a proton [39]. The adsorption of a proton results in the transfer of an electron through the circuit according to the reaction $M+H^{+}+e^{-} \rightarrow M\text{-}H$.

It has been suggested that the hydrogenation of pyridinic-nitrogen dopants in graphitic materials can be involved in the activation of the ORR in alkaline solutions [32]. Since this process depends not only on the pH but also on the electrode potential, the hydrogenation of pyridinic nitrogen-dopants can take place actually under alkaline conditions. In fact, ORR activity on nitrogen-doped graphitic materials is usually reported under alkaline conditions [13-15, 17-19]. Thus, hydrogenated pyridinic nitrogen-dopants were also considered in the investigated configurations. Surprisingly, when the carbon atom **a** laterally adjacent to a hydrogenated pyridinic nitrogen-dopant in an armchair edge was tested for activation in the presence of an additional distant graphitic-nitrogen dopant (Fig. 1C), a very favorable monodentate chemisorbed state was found (Fig. 3). As can be observed in the geometric details displayed in Fig. 3A, significant bond changes have taken place. First, the tested carbon atom **a** is bonded to the nearest atom of the oxygen molecule (O1) at a distance of ca. 0.144 nm. In addition, the O1-O2 bond of the molecule is significantly elongated, from ca. 0.121 nm in the original O_2 molecule to ca. 0.146 nm. Finally, an extraordinarily short (ca. 0.155 nm) hydrogen bond, between O2 and the nearest hydrogen atom of the explicit water molecule is formed. The described chemisorbed state is favorable by ca. 1.76 eV and stable by ca. 0.63 eV (Fig. 2). To better understand the found chemisorbed state, the electrostatic potential mapped on the electron isodensity surface $\rho = 0.01$ e/Å^3 was visualized (Fig. 3B). The corresponding Mulliken

ACCEPTED MANUSCRIPT

partial charges are also provided in Fig. 3C. Jointly, Figs. 3B and 3C describe charge concentration in O1 (ca. -0.30 e^-) and mainly O2 (ca. -0.58 e^-), which is partially contributed from the region corresponding to the distant graphitic nitrogen-dopant. This excess of charge stands for ca. 0.88 e^- for the whole of the molecule, indicating that the adsorbed oxygen species would have superoxide characteristics, which is always regarded as the first step in the reduction process. The mentioned excess of charge would be stabilized by pairing in spin with the unpaired electron, originated in the oxygen molecule because of loss of the double bond characteristics, and by the solvation effect [22].

To understand the role of the additional graphitic nitrogen-dopant in the stabilization of the adsorbed species, this nitrogen atom was substituted by a carbon atom in the model to determine whether a stable adsorbed state was found (Fig. 1D). When the same laterally adjacent carbon atom was tested for activation (**a** in Fig. 1D), a significant monodentate chemisorbed state was found, which is less stable than the previously described one (Fig. 2). Geometry, electrostatic potential map and partial charges are provided in Fig. S2. This last chemisorbed state would be weakened by the lack of charge that the region corresponding to the graphitic nitrogen-dopant was providing in the previous model. When the geometries and charges of both found chemisorbed states are compared (Figs. 3 and S2), it can be seen that negative charge excess and the bond distances are comparable, indicating the formation of a chemisorbed species with a superoxide characteristic. Thus, it can be concluded from Fig. 2, that hydrogenated pyridinic-nitrogen dopants at armchair edges of graphitic materials would give rise to clearly favorable chemisorbed states of molecular oxygen on their laterally adjacent carbon atoms. In addition, that only when pyridinic nitrogen-dopants are hydrogenated the investigated chemisorbed state is clearly favorable. No additional charge would be required for activating oxygen when pyridinic nitrogen-dopants are hydrogenated. Nevertheless, extra available charge would favor the investigated mechanism.

ACCEPTED MANUSCRIPT

It could be argued that the excess of charge required for the stabilization of the adsorbed oxygen species is that which has been provided in the process of the hydrogenation, and that a system providing only available charge, and not necessarily hydrogenated, would yield a stable chemisorbed state. However, when the results corresponding to the model displayed in Fig. 1A are compared to those corresponding to Fig. 1B, in which available charge is provided by an additional graphitic nitrogen-dopant, it is evident that both chemisorbed states present a similar stability (Fig. 2). This fact clearly indicates that the chemical changes brought about by the hydrogenation process are responsible of the stabilization of the investigated chemisorbed state, and that additional available charge further favors the mechanism.

The carbon atom inwardly adjacent to the pyridinic nitrogen-dopant (labeled as **b** in Fig. 1) was also tested for activation. However, for reasons that will be better understood later, a much less significant chemisorbed state was found. For clarity, those results are omitted. All these facts suggest that the ORR can be activated by means of the adsorption of oxygen in form of a superoxide on a carbon atom adjacent to a hydrogenated pyridinic nitrogen-dopant at an armchair edge of graphitic materials. The next step would be the formation of an adsorbed peroxide species, facilitated by the short O2-H distance in the hydrogen bond, with the concomitant transfer of an electron. From that point, the proposed mechanisms [23] do not differ significantly from those proposed for metals [21]. Regarding the favorable nature of the investigated ORR activation mechanism, it is known that adsorption energies of the intermediate species should have an ideal value so that the reaction rate is maximized. Deviations from that ideal value lead to a diminution of the activity and gives rise to the typical volcano curves [40]. The situation for the ORR is more complex, since several adsorbed species are involved, whose adsorption energies should be optimized. However, it is generally accepted that the adsorption energies of the different intermediates in the ORR follow scaling relationships [24, 41], so that the adsorption energies of the different adsorbed species are

ACCEPTED MANUSCRIPT

directly proportional. Thus, simple volcano curves can be obtained even for this complex reaction. For graphene compounds, the adsorption energies for the intermediates on pristine materials are very low and the doping leads to moderate increases in these energies. Thus, the values obtained here would be in the rising branch of the volcano curve, for which an increase of the stabilization energy leads to increases in the activity of the material.

To understand why the hydrogenation of pyridinic nitrogen-dopants at armchair edges so clearly favor the activation of molecular oxygen on graphitic materials, two details are discussed (Fig. 4). On one hand, it can be observed in Fig. 4A that, before activation, the hydrogenated pyridinic nitrogen-dopant is coplanar within the surface. Planarity is a signature of the sp^2 hybridization. Thus, after hydrogenation, the pyridinic nitrogen-dopant would retain its graphitic character. So, the corresponding bonding structure could be described as a proton bonded to the lone pair exposed by the pyridinic nitrogen-dopant and an additional neutralizing electron spread out on the surface, including the region polarized by the proton. Therefore, the formation of a covalent bond between the nitrogen and the proton, with the participation of the neutralizing charge, would not be favorable enough as for breaking the over-stabilized aromatic structure. The above description can be verified by comparing the electrostatic potentials mapped on electron isodensity surfaces, and the partial charges, before and after the hydrogenation process (Fig. 5). After the hydrogenation process, a segregated charge distribution, with positive character in the region corresponding to the hydrogenated pyridinic nitrogen-dopant and charge spread out on the surface, can be inferred from Figs. 5C-D.

On the other hand, it can be observed in Fig. 4B that, after activation, both the nitrogen dopant and the carbon atom enabling the activation are displaced out of the plane, in opposite directions, occupying each one of them the center of the respective tetrahedron defined by the atoms they are bonded to. Obviously, for nitrogen, a vertex is missing. The tetrahedral disposition is a signature of the sp^3 hybridization. Therefore, it can be concluded that, to activate

ACCEPTED MANUSCRIPT

molecular oxygen under the considered mechanism, both the nitrogen dopant and the carbon atom enabling the activation would switch from the sp^2 hybridization state to sp^3. Moreover, from the energetics point of view, chemisorption requires a bonding restructuration of both adsorbent and adsorbate, taking place only if this is energetically favorable. On one hand, a suboptimal reactant reference is established because the proton captured by the pyridinic nitrogen-dopant and the neutralizing electron taken from the circuit remain segregated. On the other hand, the proton captured by the pyridinic nitrogen-dopant and the neutralizing electron provide additional restructuring possibilities. Being the adsorbent an over-stabilized aromatic surface, a confined restructuration, enabling the chemisorption, would allow retaining aromaticity, increasing the feasibility of the reaction. On a carbon atom laterally adjacent to a hydrogenated pyridinic nitrogen-dopant at an armchair edge (carbon atom **a** in Figs. 1C-D), a bonding configuration enabling the investigated chemisorption can be achieved by means of a very much localized restructuring of the surface (Fig. 4B), losing very little aromatic energy. By contrast, when the carbon atom inwardly adjacent to a hydrogenated pyridinic nitrogen-dopant at an armchair edge (carbon atom **b** in Figs. 1C-D) is considered for activation, a broader surface restructuration is needed. In this restructuration, much more aromatic energy is lost, giving rise to a much less favorable chemisorbed state. Similar considerations apply to the activation on carbon atoms adjacent to non-hydrogenated pyridinic nitrogen-dopants, even when extra available charge is provided. Moreover, chemisorption at the edge can be better relaxed without the eventual opposition of parts that may try to impose other geometry. For the chemisorbed state displayed in Fig. 3, after chemisorption, a virtually undistorted surface can be observed in Fig. 3A. Finally, once the monodentate chemisorption is sufficiently favorable, as more charge is available, more charge can be paired to the unpaired electron until reaching a limit, lowering the energy. In addition, given that the excess of charge in the oxygen is stabilized by the solvation effect [22], as more charge is paired to the unpaired electron, more

ACCEPTED MANUSCRIPT

solvation energy is generated, favoring even more the mechanism. Thus, the main role of non-hydrogenated pyridinic nitrogen-dopants would be precursor of the truly relevant hydrogenated state. As a conclusion, the monodentate activation of molecular oxygen at armchair edges of nitrogen-doped graphitic materials would be enabled by the hydrogenation of the pyridinic nitrogen-dopants and driven by the available charge.

The above discussion about the Fig. 4A suggests that hydrogenated pyridinic nitrogen-dopants could play an additional role to destabilizing their adjacent carbons. Given that the formation of a covalent bond between the pyridinic nitrogen-dopant and hydrogen would not be favorable enough as for breaking the aromatic structure, it was supposed that charge supplied in the hydrogenation of the pyridinic nitrogen-dopants may become available, eventually contributing to intensifying the investigated mechanism on a distant site. This was the case observed in a graphene structure containing two distant nitrogen graphitic-dopants [22]. One nitrogen dopant is providing the additional charge required for the process and the second one is destabilizing the adjacent carbon atoms to facilitate the chemisorption. To verify the hypothesis and using the models introduced in Figs. 1B-C, the monodentate chemisorption of molecular oxygen on a carbon atom adjacent to the graphitic-nitrogen dopant (labeled as **c** in Figs. 1B-C) was investigated under the two possible hydrogenation states of the pyridinic nitrogen-dopant. The corresponding reaction paths are displayed in Fig. 6. Only when the pyridinic nitrogen-dopant was hydrogenated, a sufficiently significant chemisorbed state was found on the carbon atom adjacent to the graphitic nitrogen-dopant (Fig 7). It can be concluded from Fig. 7 that hydrogenated pyridinic nitrogen-dopants would provide available charge, contributing to drive the investigated mechanism on other carbons sites, even not those directly bonded to the nitrogen. In any case, as can be also observed in Fig. 6, the considered activation on the carbon atom **a** laterally adjacent to the hydrogenated pyridinic nitrogen-dopant would be, by far, the most favorable.

ACCEPTED MANUSCRIPT

The described effects suggest that the activation of the ORR could take place as soon as the pyridinic nitrogen-dopant has been hydrogenated. The potential at which this process can take place can be estimated using the approach introduced by Anderson and col. [42, 43], which uses the strength of the N-H bond and the standard redox potential for the reaction $H^+(aq)+e = H(aq)$. Depending on the specific configuration of the nitrogen dopants and the inclusion of solvent effects on the calculations, the estimated standard potential for the hydrogenation process varies between 0.2 and 0.7 V (SHE). This means that the hydrogenation process would take place between 0.2 and 0.7 V in the RHE scale, which is in agreement with the potential region where the activation of the reaction takes place experimentally. These values would imply that the considered activation process could take place both in acidic and alkaline solutions. However, the experimental results indicate that these materials are active for the ORR manly under alkaline conditions. Different steps in the complex ORR could be activated or hindered as an exclusive effect of the pH, affecting the whole reaction. Additionally, water structure and electrode charge depends on the pH, which can also affect the reactivity of the whole process. For instance, the reactivity for the ORR on Pt single crystal electrodes is significantly different in alkaline and acidic solutions, while the different adsorbates involved in the reaction do not seem significantly affected by pH changes, as revealed by the similar voltammograms obtained in the absence of oxygen in perchloric and sodium hydroxide solutions [44, 45].

The role played by pyridinic nitrogen-dopants at zigzag edges in the considered activation was also investigated. Therefore, a new set of calculations, completely analogous to the one already performed for the armchair case, was conducted for the configurations displayed in Fig. 8. A similar chemisorbed state to the one displayed in Fig. 3 can be observed in Fig. S3. However, the resulting state is much less favorable and much less stable because a strictly

ACCEPTED MANUSCRIPT

localized restructuring of the surface enabling the chemisorption is not possible in this case (carbon atom **a** in Fig. 8C). Once more, only when the pyridinic nitrogen-dopant was hydrogenated, a sufficiently significant chemisorbed state was found on the carbon atom adjacent to the graphitic-nitrogen dopant (Fig. S5). However, the comparisons between Fig. 7 and S5 and between Fig. 5 and S6 suggest that the charge involved in the hydrogenation of pyridinic nitrogen-dopants located at zigzag edges would be slightly less segregated and would become slightly less available than in the case of armchair edges.

Finally, the role played by graphitic nitrogen-dopants in the investigated reaction is briefly revisited. In our previous communication [22], computational evidences that graphitic nitrogen-dopants would be capable of locally destabilizing carbon atoms and globally providing available charge were provided. In fact, the capability of contributing with charge of graphitic nitrogen-dopants has been corroborated here. However, the reasons explaining why graphitic nitrogen-dopants exhibit the described capabilities have not been yet clarified. It is known that substitutional nitrogen-dopants give rise to n-type graphene, altering the DOS and providing charge [30, 46]. In addition, we propose here chemical explanations. The highly stabilized state reached by the collective nature of the sp^2 hybridized network in graphene would be significantly destabilized if a graphitic nitrogen-dopant contributed to the bonding network with only the three electrons of valence. This fact would explain the relative advantage of unpairing the 2s electrons of nitrogen in different molecular orbitals, giving rise to a pentavalent behavior. Moreover, the higher electronegativity of nitrogen with respect to carbon would concentrate the paired charge implicated in the bonding network closer to the nitrogen atom. Finally, part of the charge related to the unpaired electrons would be made available to the adjacent carbon atoms and spread out on the surface, to compensate partially the excess of charge located close to the nitrogen. This spread out charge would be available to activate the chemisorption of oxygen in specific carbon atoms. In order to support the given explanation, the electron density

ACCEPTED MANUSCRIPT

difference between a periodic model of nitrogen-doped graphene and the same model with the nitrogen atom substituted by a carbon atom was visualized (Fig. 10). Fig.10 is completely consistent with the above description, since it shows high charge concentration on the nitrogen atom core (Fig. 10A) and small charge distribution over the carbon network, avoiding the nitrogen atom region (Fig. 10C). Additionally, the pentavalent behavior provides an explanation for the fact that graphitic nitrogen-dopants favor the activation of their adjacent carbon atoms. For activating molecular oxygen by means of chemisorption, the involved carbon atom has to switch from sp^2 hybridization to sp^3. On a carbon atom adjacent to a graphitic nitrogen-dopant, its transition from sp^2 to sp^3 can be accompanied by a switch in the nitrogen-dopant role from pentavalent to trivalent, in sp^3 mode. By switching from the pentavalent to the trivalent behavior, the energy leaked unpairing the 2s electrons is recovered, enabling a favorable chemisorbed state.

4. Conclusions

Nitrogen-doped graphitic materials favor ORR, though sites and mechanisms are under discussion. To favor the monodentate chemisorption of molecular oxygen on these materials locally destabilized carbon atoms and globally available charge would be required. In a previous work [22], we provided computational evidence that unclustered graphitic nitrogen-dopants would be capable of both, locally destabilizing carbon atoms and globally providing available charge, enabling significant monodentate chemisorbed states of molecular oxygen in the basal plane. And, here, we have provided computational evidence that hydrogenated pyridinic nitrogen-dopants, mainly at armchair edges, would be also capable of both, locally destabilizing carbon atoms and globally providing available charge, enabling significant monodentate chemisorbed states of molecular oxygen at the edges. Moreover, it has been shown that charge provided by graphitic nitrogen-dopants in the basal plane would favor the activation at the

ACCEPTED MANUSCRIPT

edges. Meanwhile, the charge required for the hydrogenation of the pyridinic nitrogen-dopants at the edges would favor the activation in the basal plane. In addition, the stabilizing role played by the solvation effect in the investigated mechanism should not be forgotten. In any case, the monodentate chemisorption of molecular oxygen on carbon atoms laterally adjacent to hydrogenated pyridinic nitrogen-dopants at armchair edges would be, by far, the most favorable. By contrast, the chemisorbed state of oxygen is much less favorable when the hydrogenated pyridinic nitrogen-dopants are located at zigzag edges. Likewise, non-hydrogenated pyridinic nitrogen-dopants would not be capable of favoring the monodentate activation of molecular oxygen in any considered way. Thus, from the point of view of the investigated mechanism, the main role played by non-hydrogenated pyridinic nitrogen-dopants would be precursor of the truly relevant hydrogenated state. Therefore, the monodentate activation of molecular oxygen on optimal nitrogen-doped graphitic materials would be enabled by hydrogenation and driven by the available charge. The identified activation mechanism should take place in the same potential region where the hydrogenation process takes place, as has been already observed experimentally [32]. By focusing on the monodentate activation, fundamental effects would have been brought to light, explaining the experimental observations originating this research, and enabling the discussion of different configurations. The effects and mechanisms here described have been verified using different hydrogen-passivated molecular and periodic models of nitrogen-doped graphene, and armchair and zigzag graphene nanoribbons and single-walled carbon nanotubes (Fig. S7). Thus, the insights here provided should be useful in the performance evaluation and design optimization of a broad range of nitrogen-containing graphitic materials, such as graphitic carbon nitrides, graphitic nitrogen-containing COFs or graphitic boron-carbon-nitrogen ternary systems.

ACCEPTED MANUSCRIPT

Acknowledgments

This work has been financially supported by the MICINN (Spain) (project 2013-44083-P) and Generalitat Valenciana (project PROMETEOII/2014/013).

References

[1] M. Winter, R.J. Brodd, What Are Batteries, Fuel Cells, and Supercapacitors?, Chem. Rev., 104 (2004) 4245-4270.

[2] Y. Bing, H. Liu, L. Zhang, D. Ghosh, J. Zhang, Nanostructured Pt-alloy electrocatalysts for PEM fuel cell oxygen reduction reaction, Chem. Soc. Rev., 39 (2010) 2184-2202.

[3] A. Morozan, B. Jousselme, S. Palacin, Low-platinum and platinum-free catalysts for the oxygen reduction reaction at fuel cell cathodes, Energy Environ. Sci., 4 (2011) 1238-1254.

[4] K.A. Kuttiyiel, K. Sasaki, Y. Choi, D. Su, P. Liu, R.R. Adzic, Bimetallic IrNi core platinum monolayer shell electrocatalysts for the oxygen reduction reaction, Energy Environ. Sci., 5 (2012) 5297-5304.

[5] I.E.L. Stephens, A.S. Bondarenko, U. Gronbjerg, J. Rossmeisl, I. Chorkendorff, Understanding the electrocatalysis of oxygen reduction on platinum and its alloys, Energy Environ. Sci., 5 (2012) 6744-6762.

[6] M. Lefevre, E. Proietti, F. Jaouen, J.P. Dodelet, Iron-Based Catalysts with Improved Oxygen Reduction Activity in Polymer Electrolyte Fuel Cells, Science, 324 (2009) 71-74.

[7] F. Jaouen, E. Proietti, M. Lefevre, R. Chenitz, J.-P. Dodelet, G. Wu, H.T. Chung, C.M. Johnston, P. Zelenay, Recent advances in non-precious metal catalysis for oxygen-reduction reaction in polymer electrolyte fuel cells, Energy Environ. Sci., 4 (2011) 114-130.

[8] Z.W. Chen, D. Higgins, A.P. Yu, L. Zhang, J.J. Zhang, A review on non-precious metal electrocatalysts for PEM fuel cells, Energy Environ. Sci., 4 (2011) 3167-3192.

[9] K. Strickland, E. Miner, Q. Jia, U. Tylus, N. Ramaswamy, W. Liang, M.-T. Sougrati, F. Jaouen, S. Mukerjee, Highly active oxygen reduction non-platinum group metal electrocatalyst without direct metal-nitrogen coordination, Nat Commun, 6 (2015).

[10] D.-W. Wang, D. Su, Heterogeneous nanocarbon materials for oxygen reduction reaction, Energy Environ. Sci., 7 (2014) 576-591.

[11] X.-K. Kong, C.-L. Chen, Q.-W. Chen, Doped graphene for metal-free catalysis, Chem. Soc. Rev., 43 (2014) 2841-2857.

[12] L. Dai, Y. Xue, L. Qu, H.-J. Choi, J.-B. Baek, Metal-Free Catalysts for Oxygen Reduction Reaction, Chem. Rev., 115 (2015) 4823-4892.

[13] K. Gong, F. Du, Z. Xia, M. Durstock, L. Dai, Nitrogen-Doped Carbon Nanotube Arrays with High Electrocatalytic Activity for Oxygen Reduction, Science, 323 (2009) 760-764.

[14] L. Qu, Y. Liu, J.-B. Baek, L. Dai, Nitrogen-Doped Graphene as Efficient Metal-Free Electrocatalyst for Oxygen Reduction in Fuel Cells, ACS Nano, 4 (2010) 1321-1326.

ACCEPTED MANUSCRIPT

[15] Z. Wang, R. Jia, J. Zheng, J. Zhao, L. Li, J. Song, Z. Zhu, Nitrogen-Promoted Self-Assembly of N-Doped Carbon Nanotubes and Their Intrinsic Catalysis for Oxygen Reduction in Fuel Cells, ACS Nano, 5 (2011) 1677-1684.

[16] H. Wang, T. Maiyalagan, X. Wang, Review on Recent Progress in Nitrogen-Doped Graphene: Synthesis, Characterization, and Its Potential Applications, ACS Catal., 2 (2012) 781-794.

[17] L. Lai, J.R. Potts, D. Zhan, L. Wang, C.K. Poh, C. Tang, H. Gong, Z. Shen, J. Lin, R.S. Ruoff, Exploration of the active center structure of nitrogen-doped graphene-based catalysts for oxygen reduction reaction, Energy Environ. Sci., 5 (2012) 7936-7942.

[18] T. Sharifi, G. Hu, X. Jia, T. Wågberg, Formation of Active Sites for Oxygen Reduction Reactions by Transformation of Nitrogen Functionalities in Nitrogen-Doped Carbon Nanotubes, ACS Nano, 6 (2012) 8904-8912.

[19] T. Xing, Y. Zheng, L.H. Li, B.C.C. Cowie, D. Gunzelmann, S.Z. Qiao, S. Huang, Y. Chen, Observation of Active Sites for Oxygen Reduction Reaction on Nitrogen-Doped Multilayer Graphene, ACS Nano, 8 (2014) 6856-6862.

[20] C.H. Choi, H.-K. Lim, M.W. Chung, J.C. Park, H. Shin, H. Kim, S.I. Woo, Long-Range Electron Transfer over Graphene-Based Catalyst for High-Performing Oxygen Reduction Reactions: Importance of Size, N-doping, and Metallic Impurities, J. Am. Chem. Soc., 136 (2014) 9070-9077.

[21] R.R. Adzic, Recent advances in the kinetics of oxygen reduction, in: J. Lipkowski, P.N. Ross (Eds.) Electrocatalysis, Wiley-VCH, New York, 1998, pp. 197-242.

[22] A. Ferre-Vilaplana, E. Herrero, Charge transfer, bonding conditioning and solvation effect in the activation of the oxygen reduction reaction on unclustered graphitic-nitrogen-doped graphene, Phys. Chem. Chem. Phys., 17 (2015) 16238-16242.

[23] L. Yu, X. Pan, X. Cao, P. Hu, X. Bao, Oxygen reduction reaction mechanism on nitrogen-doped graphene: A density functional theory study, J. Catal., 282 (2011) 183-190.

[24] Y. Jiao, Y. Zheng, M. Jaroniec, S.Z. Qiao, Origin of the Electrocatalytic Oxygen Reduction Activity of Graphene-Based Catalysts: A Roadmap to Achieve the Best Performance, J. Am. Chem. Soc., 136 (2014) 4394-4403.

[25] S. Yang, G.-L. Zhao, E. Khosravi, First Principles Studies of Nitrogen Doped Carbon Nanotubes for Dioxygen Reduction, J. Phys. Chem. c, 114 (2010) 3371-3375.

[26] L. Zhang, Z. Xia, Mechanisms of Oxygen Reduction Reaction on Nitrogen-Doped Graphene for Fuel Cells, J. Phys. Chem. c, 115 (2011) 11170-11176.

[27] D.W. Boukhvalov, Y.-W. Son, Oxygen reduction reactions on pure and nitrogen-doped graphene: a first-principles modeling, Nanoscale, 4 (2012) 417-420.

[28] S. Ni, Z. Li, J. Yang, Oxygen molecule dissociation on carbon nanostructures with different types of nitrogen doping, Nanoscale, 4 (2012) 1184-1189.

[29] L. Zhao, R. He, K.T. Rim, T. Schiros, K.S. Kim, H. Zhou, C. Gutiérrez, S.P. Chockalingam, C.J. Arguello, L. Pálová, D. Nordlund, M.S. Hybertsen, D.R. Reichman, T.F. Heinz, P. Kim, A. Pinczuk, G.W. Flynn, A.N. Pasupathy, Visualizing Individual Nitrogen Dopants in Monolayer Graphene, Science, 333 (2011) 999-1003.

[30] R. Lv, Q. Li, A.R. Botello-Méndez, T. Hayashi, B. Wang, A. Berkdemir, Q. Hao, A.L. Elías, R. Cruz-Silva, H.R. Gutiérrez, Y.A. Kim, H. Muramatsu, J. Zhu, M. Endo, H. Terrones,

ACCEPTED MANUSCRIPT

J.-C. Charlier, M. Pan, M. Terrones, Nitrogen-doped graphene: beyond single substitution and enhanced molecular sensing, Sci Rep-Uk, 2 (2012) 586.

[31] H. Kim, K. Lee, S.I. Woo, Y. Jung, On the mechanism of enhanced oxygen reduction reaction in nitrogen-doped graphene nanoribbons, Phys. Chem. Chem. Phys., 13 (2011) 17505-17510.

[32] Q. Li, B.W. Noffke, Y. Wang, B. Menezes, D.G. Peters, K. Raghavachari, L.-s. Li, Electrocatalytic Oxygen Activation by Carbanion Intermediates of Nitrogen-Doped Graphitic Carbon, J. Am. Chem. Soc., 136 (2014) 3358-3361.

[33] J.P. Perdew, K. Burke, M. Ernzerhof, Generalized Gradient Approximation Made Simple, Phys. Rev. Lett., 77 (1996) 3865-3868.

[34] B. Delley, An all-electron numerical method for solving the local density functional for polyatomic molecules, J. Chem. Phys., 92 (1990) 508-517.

[35] B. Delley, From molecules to solids with the DMol(3) approach, J. Chem. Phys., 113 (2000) 7756-7764.

[36] B. Delley, The conductor-like screening model for polymers and surfaces, Mol. Simul., 32 (2006) 117-123.

[37] A. Tkatchenko, M. Scheffler, Accurate Molecular Van Der Waals Interactions from Ground-State Electron Density and Free-Atom Reference Data, Phys. Rev. Lett., 102 (2009) 073005.

[38] S. Grimme, Semiempirical GGA-type density functional constructed with a long-range dispersion correction, J. Comput. Chem., 27 (2006) 1787-1799.

[39] B.E. Conway, B.V. Tilak, Interfacial processes involving electrocatalytic evolution and oxidation of H2, and the role of chemisorbed H, Electrochim. Acta, 47 (2002) 3571-3594.

[40] S. Trasatti, Work function, electronegativity, and electrochemical behaviour of metals: III. Electrolytic hydrogen evolution in acid solutions, J. Electroanal. Chem., 39 (1972) 163-184.

[41] V. Tripković, E. Skúlason, S. Siahrostami, J.K. Nørskov, J. Rossmeisl, The oxygen reduction reaction mechanism on Pt(1 1 1) from density functional theory calculations, Electrochim. Acta, 55 (2010) 7975-7981.

[42] R.A. Sidik, A.B. Anderson, N.P. Subramanian, S.P. Kumaraguru, B.N. Popov, O2 Reduction on Graphite and Nitrogen-Doped Graphite: Experiment and Theory, J. Phys. Chem. B, 110 (2006) 1787-1793.

[43] K.A. Kurak, A.B. Anderson, Nitrogen-Treated Graphite and Oxygen Electroreduction on Pyridinic Edge Sites, J. Phys. Chem. c, 113 (2009) 6730-6734.

[44] R. Rizo, E. Herrero, J.M. Feliu, Oxygen reduction reaction on stepped platinum surfaces in alkaline media, Phys. Chem. Chem. Phys., 15 (2013) 15416-15425.

[45] R. Rizo, E. Sitta, E. Herrero, V. Climent, J.M. Feliu, Towards the understanding of the interfacial pH scale at Pt(111) electrodes, Electrochim. Acta, 162 (2015) 138-145.

[46] D. Wei, Y. Liu, Y. Wang, H. Zhang, L. Huang, G. Yu, Synthesis of N-Doped Graphene by Chemical Vapor Deposition and Its Electrical Properties, Nano Lett., 9 (2009) 1752-1758.

ACCEPTED MANUSCRIPT

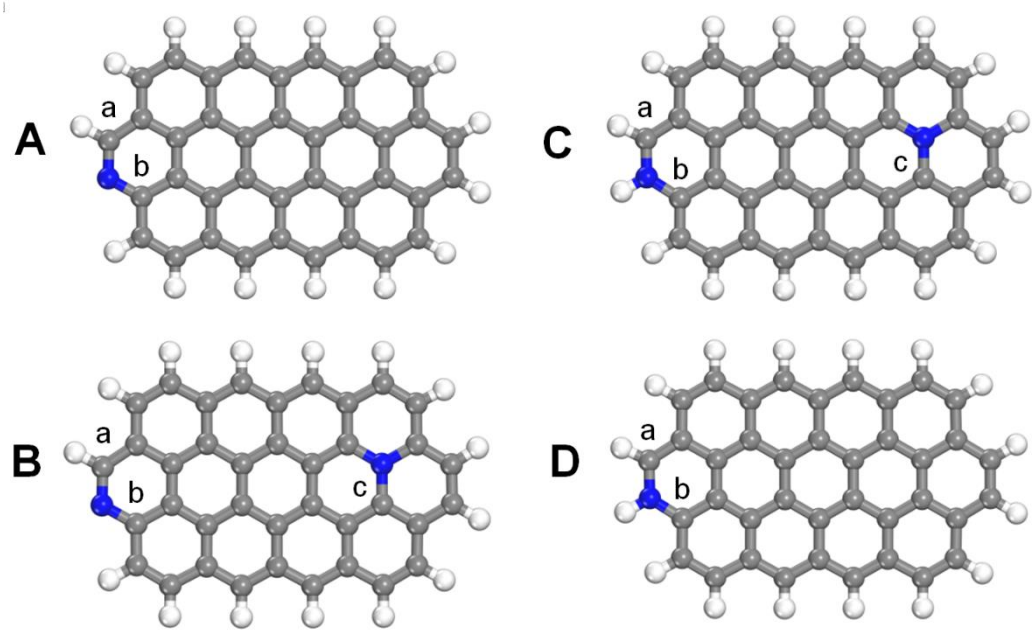

Figure 1. Different unclustered nitrogen dopants configurations with a pyridinic nitrogen-dopant located at an armchair edge: (A) A single nitrogen dopant in a pyridinic form. (B) A pyridinic nitrogen-dopant in addition to a distant graphitic one. (C) A hydrogenated pyridinic nitrogen-dopant in addition to a distant graphitic one. (D) A single nitrogen dopant in a hydrogenated pyridinic form.

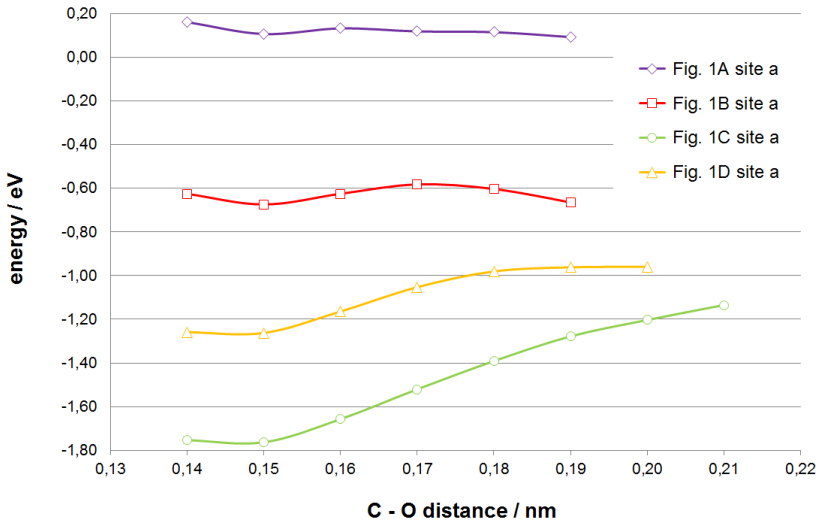

Figure 2. Total energies, referred to their respective references (adsorbent energy plus that corresponding to the adsorbate complex in the bulk), for an oxygen molecule located on top of the carbon atom **a**, for the different configurations displayed in Fig. 1, estimated at different constrained distances between the carbon atom and the nearest oxygen atom of the molecule. Five explicit water molecules in addition to a continuum model were used as solvation effect treatment (Fig. S1).

ACCEPTED MANUSCRIPT

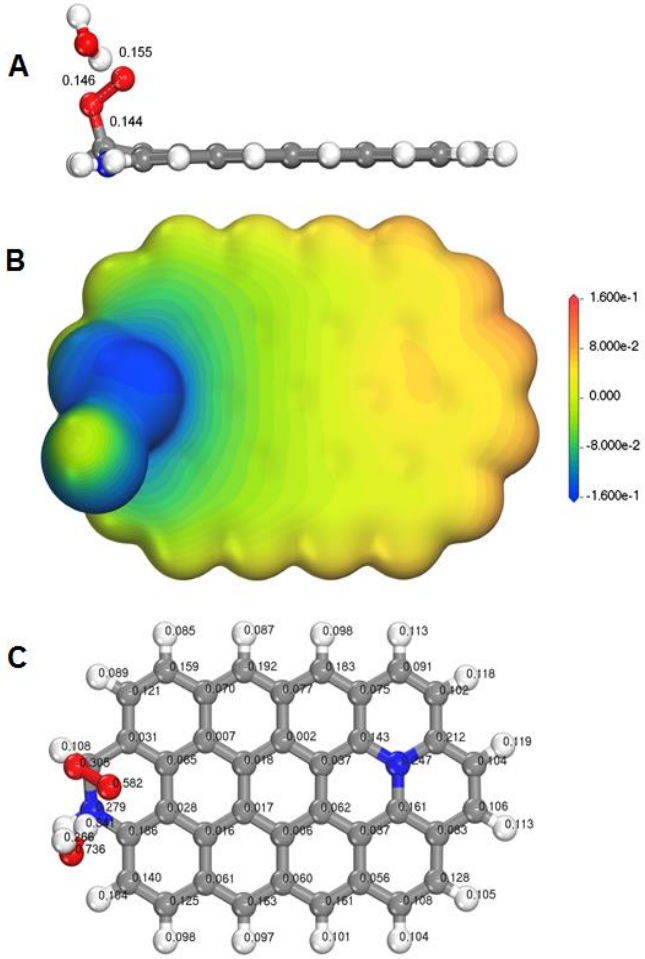

Figure 3. Monodentate chemisorbed state of molecular oxygen on the carbon atom **a** of the configuration displayed as Fig. 1C. An explicit water molecule in addition to a continuum model was used as solvation effect treatment. (A) Adsorbent-adsorbate-solvent geometry (distances in nm). (B) Electrostatic potential in Ha/e^- mapped on the electron isodensity surface $\rho = 10\ e^-\ nm^{-3}$. (C) Mulliken partial charges in e^-.

ACCEPTED MANUSCRIPT

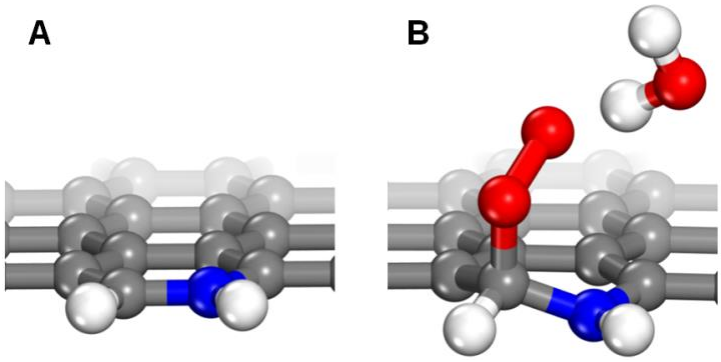

Figure 4. (A) Geometric detail of the surface model displayed as Fig. 1C. (B) Geometric detail of the chemisorbed state displayed in Fig. 3

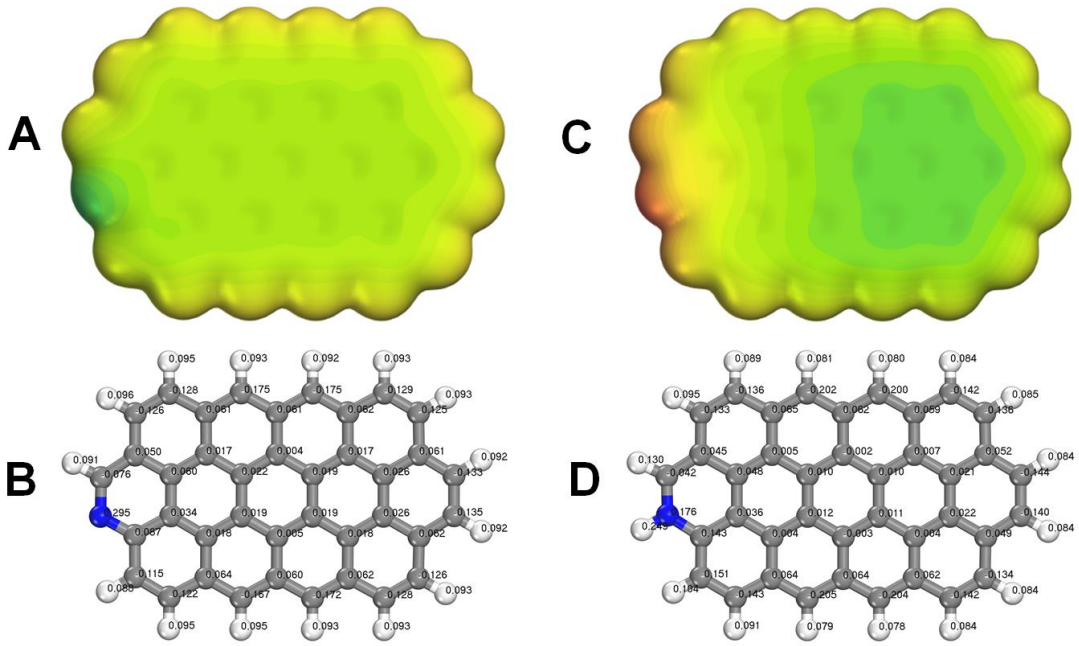

Figure 5. Charge distributions of the molecular model of nitrogen-doped graphene displayed as Fig. 1A, before (A and B) and after (C and D) the hydrogenation process. Panels A and C. Electrostatic potential in Ha/e^- on the electron isodensity surface $\rho = 10\ e^-/nm^3$, using the same color map as in Fig. 3. Panels B and D. Mulliken partial charges in e^-.

ACCEPTED MANUSCRIPT

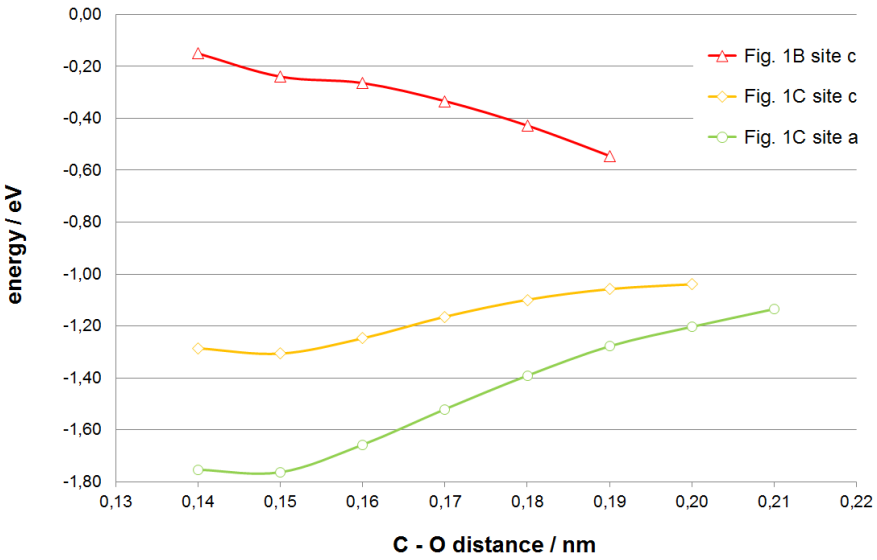

Figure 6. Total energies, referred to their respective references (adsorbent energy plus that corresponding to the adsorbate complex in the bulk), for an oxygen molecule located on top of the carbon atom **c**, for the configurations displayed in Figs. 1B-C, estimated at different constrained distances between the carbon atom and the nearest oxygen atom of the molecule. Five explicit water molecules in addition to a continuum model were used as solvation effect treatment (Fig. S1).The curve corresponding to the chemisorption introduced in Fig. 3 is also included for comparison.

ACCEPTED MANUSCRIPT

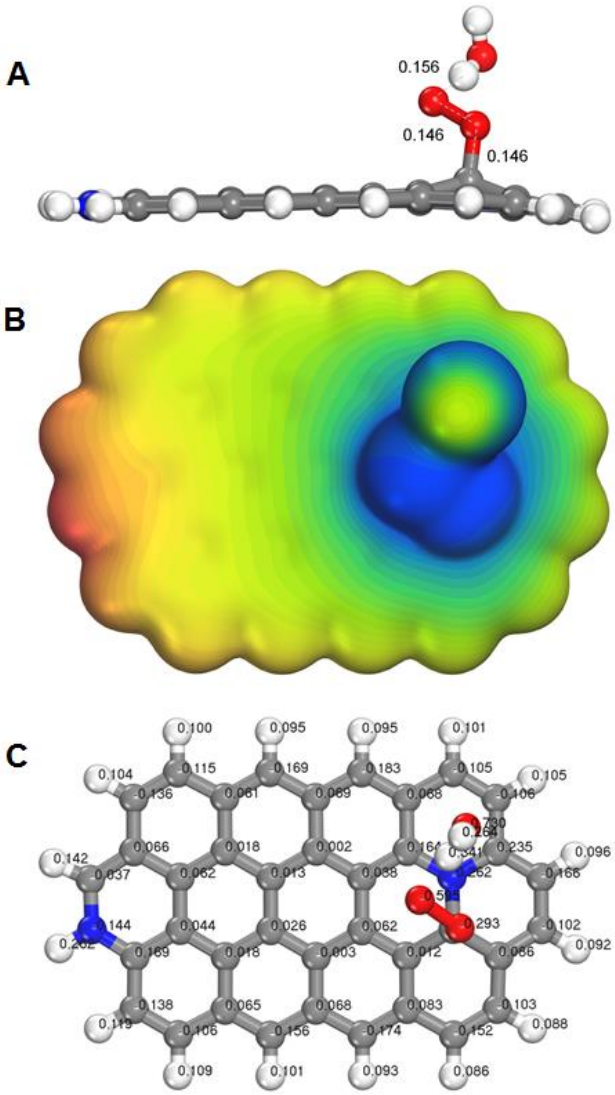

Figure 7. Monodentate chemisorbed state of molecular oxygen on the carbon atom **c** of the configuration displayed as Fig. 1C. An explicit water molecule in addition to a continuum model was used as solvation effect treatment. (A) Adsorbent-adsorbate-solvent geometry (distances in nm). (B) Electrostatic potential in Ha/e^- mapped on the electron isodensity surface $\rho = 10\ e^-\ nm^{-3}$, using the same color map as in Fig. 3. (C) Mulliken partial charges in e^-.

ACCEPTED MANUSCRIPT

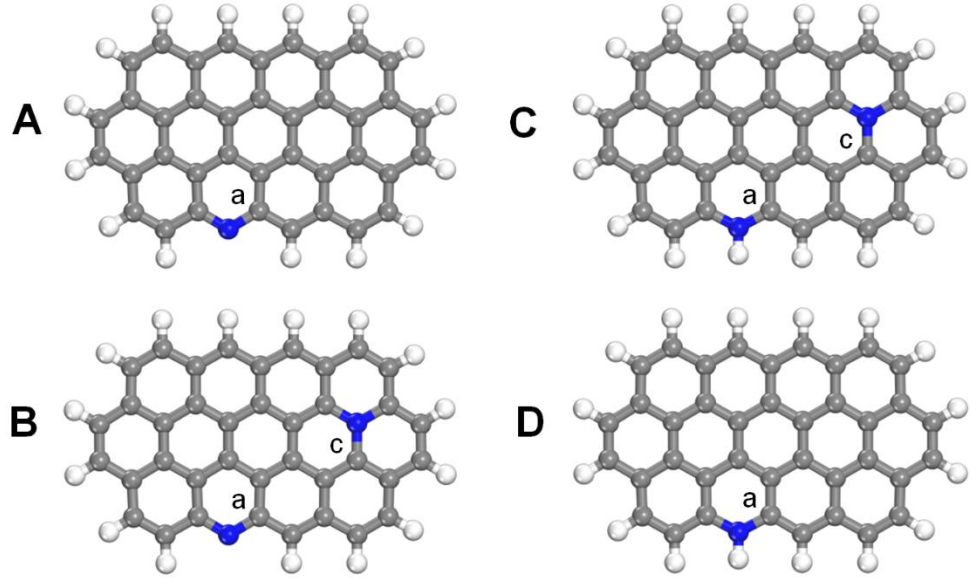

Figure 8. Different unclustered nitrogen dopants configurations with a pyridinic-nitrogen dopant located at a zig-zag edge: (A) A single nitrogen dopant in a pyridinic form. (B) A pyridinic nitrogen-dopant in addition to a distant graphitic one. (C) A hydrogenated pyridinic nitrogen-dopant in addition to a distant graphitic one. (D) A single nitrogen dopant in a hydrogenated pyridinic form.

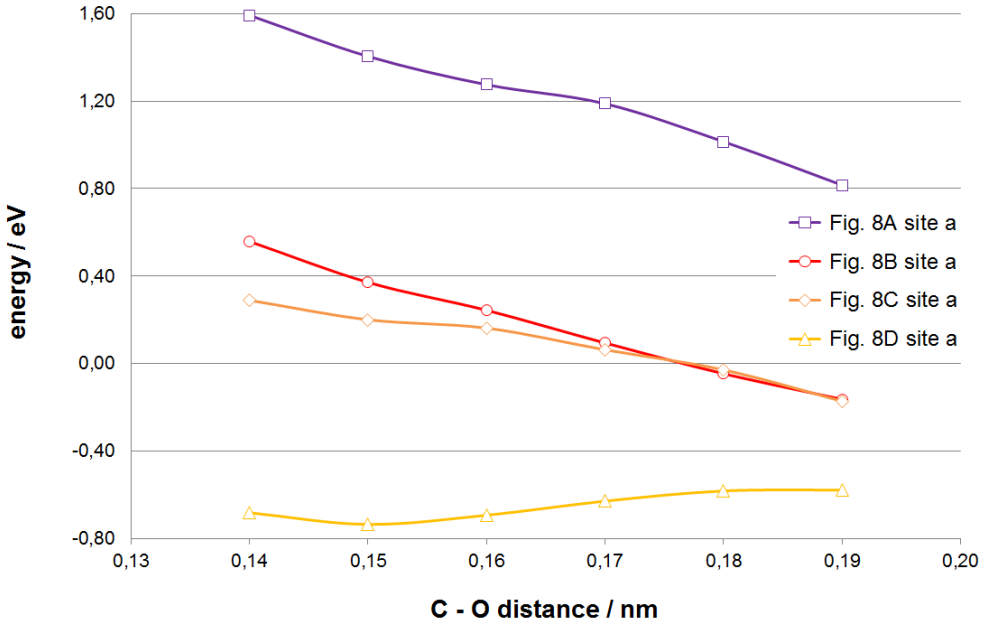

Figure 9. Total energies, referred to their respective references (adsorbent energy plus that corresponding to the adsorbate complex in the bulk), for an oxygen molecule located on top of the carbon atom **a**, for the different configurations displayed in Fig. 8, estimated at different constrained distances between the carbon atom and the nearest oxygen atom of the molecule. Five explicit water molecules in addition to a continuum model were used as solvation effect treatment (Fig. S1).

ACCEPTED MANUSCRIPT

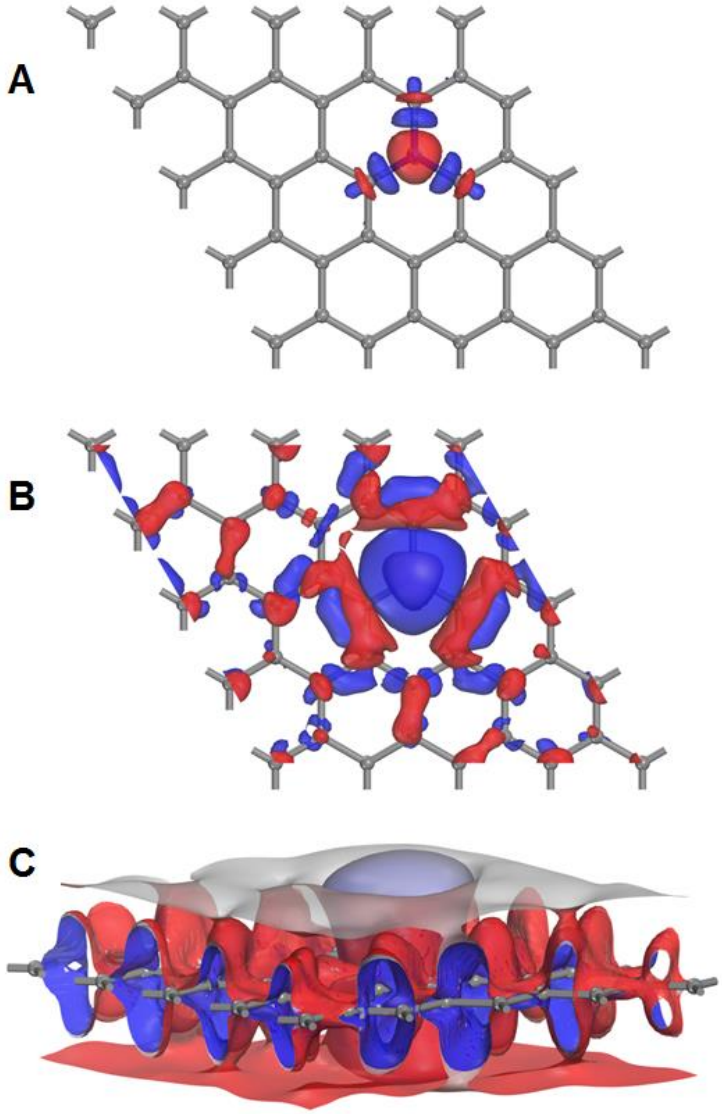

Figure 10. Electron density difference between a periodic model of nitrogen doped graphene, which includes a single graphitic nitrogen-dopant, and the same model in which the graphitic nitrogen-dopant has been substituted by a carbon atom. The red color visualize regions of charge concentration, meanwhile the blue color visualize regions of charge depletion. The visualized isosurfaces are (A) ±50 e nm^{-3}, (B) ±5 $e^{-}nm^{-3}$ and (C) ±0.02 e^{-} nm^{-3}.